International Journal of Theoretical and Mathematical Physics 2024, 14(4): 109-120
DOI: 10.5923/j.ijtmp.20241404.01

An *ab initio* GGA+U Study of the Wurtzite Structure of ZnO for Dye-Sensitized Solar Cells Application

Irungu M. Kahura[1,*], Kiprotich Sharon[1], Winfred M. Mulwa[2]

[1]Department of Physical and Biological Sciences, Murang'a University of Technology, Murang'a, Kenya
[2]Department of Physics, Egerton University, Egerton, Kenya

Abstract Due to its wide band gap and high electron mobility, ZnO is a promising semiconductor material for dye-sensitized solar cells (DSSCs). This research utilizes ab initio density functional theory (DFT) as implemented in the Quantum ESPRESSO software. Both standard DFT and DFT+U formalism were employed to explore the structural, elastic, electronic and optical characteristics of wurtzite ZnO (W-ZnO). The optimal lattice constants $a = b$ =3.289 Å and c = 5.29032 Å were obtained in DFT calculations while in the DFT+U techniques, a=b=3.269 Å and 5.211 Å were achieved. This was found to align with prior findings in the literature but exhibiting a minor reduction during the DFT+U calculations. It was noted that W-ZnO exhibits a direct band gap at the gamma point. The calculated band gaps were determined to be 0.79 eV, 1.45 eV, and 3.19 eV for the standard DFT, DFT + U_d, and DFT + U_d + U_p calculations, respectively. From the density of state (DOS) analysis, the valence band was noted to be predominantly influenced by the O-2s, Zn-3d, and O-2p orbitals, while the conduction band was primarily governed by the O-2p and Zn-4s orbitals. The computed elastic constants, along with the bulk and shear moduli of W-ZnO conformed with stability criterion of hexagonal structures indicating that W-ZnO is mechanically stable in its ground state. Overall, W-ZnO demonstrated low absorption capacity and high transmittance within the visible spectrum, rendering it a promising candidate for applications in dye-sensitized solar cells (DSSCs).

Keywords DFT+U, DSSCs, Photoanode, Wurtzite ZnO, Structural properties

1. Introduction

Dye sensitized solar cells (DSSCs) have attracted a widespread attention in recent years as a facile renewable energy source, due to the exhaustion of non-renewable energy sources [1,2]. In addition, DSSCs are presented as a low cost alternative to the conventional solar cells. DSSCs are devised by use of wide bandgap semiconductor compounds as photoanodes, such as TiO_2, SnO_2, Nb_2O_5 and ZnO, for state-of-the-art results of DSSCs [3,4]. Among these, although TiO_2 is still desired, ZnO, due to its exemplary electron mobility and wide scope of morphological variation exhibits the optimistic candidature as a photoanode compound in DSSCs [5]. Recently, ZnO has emerged as a fascinating workhorse semiconducting metal oxide compound owing to its high optical transparency, adjustable electronic properties, ease in preparation, insignificant toxicity and low cost. This is evident from the diverse reports of ZnO being active as an acceptor compound in hybrid photovoltaics [6,7], as a semiconducting scaffold in DSSCs [8,9] as a charge transport layer in organic photovoltaics [10,11]. Additionally, ZnO is a unique compound, which possesses semiconducting and piezoelectric properties [12-14]. It is a versatile oxide semiconductor with a direct bandgap of 3.37 eV as well as 60 meV of high free extinction binding energy at room temperature [15,16]. Several recent experimental and *ab initio* studies have been reported on the fundamental properties of ZnO. Structural characterization with x-ray diffractometer (XRD) has been conducted on W-ZnO nanostructures synthesised using reflux precipitation [17,18] and sol-gel [19] experimental techniques. According to these studies, W-ZnO belongs to the p63*mc* space group having a hexagonal crystalline structure with lattice constants a=3.264Å and c=5.219 Å . Dhamodharan *et al* [20] deposited ZnO thin films using spray pyrolysis technique and investigated its optical properties by use of spectrophotometer. A direct band gap of 3.37eV as well as high optical transmittance (85-95%) in the visible region that decreased with increasing photon energy was observed in this work. Experiments can often be difficult to carry out, expensive and sometimes provide only indirect information [22]. Computational techniques are therefore at an advanced stage to supplement experimental data on the basis of a microscopic model and give insights into the basic mechanisms of interaction between atoms. Density functional theory (DFT) as a computational technique has successfully been used to describe the ground state properties of W-ZnO among many other materials.

* Corresponding author:
kahuramoses1234@gmail.com (Irungu M. Kahura)
Received: Oct. 20, 2024; Accepted: Nov. 9, 2024; Published: Nov. 12, 2024
Published online at http://journal.sapub.org/ijtmp

Various codes such as Vienna ab initio Simulation Package (VASP) [23] $WIEN_2K$ [24,25], Cambridge Sequential Total Energy Package (CASTEP) [26,27] and Quantum ESPRESSO (QE) [28] among others have been employed to implement the DFT approximations. With the use of $WIEN_2K$ in the generalized gradient approximation (GGA) formalism, Khuili *et al*., [29,30], confirmed the hexagonal structure of W-ZnO with lattice constants a=3.248Å and c= 3.222Å. A direct band gap of 0.8 eV at gamma point of symmetry was reported in this study. This was higher than 0.65eV obtained by Qing *et al* [28] using local density approximation (LDA) potentials in QE code. Lei *et al* employed the CASTEP code using GGA potentials to implement DFT in the electronic structure calculations. They observed that the valence band maximum (VBM) was occupied mainly by O-2p states while the conduction band minimum (CBM) was dominated by Zn-4s states giving a direct band gap of 0.734 eV. John and Padmavathi [31] introduced the modified Becke-Johnson (mBJ) potentials to the LDA potential in their DFT study of the optical properties of W-ZnO. A low energy loss in the visible spectrum, an absorption edge of 2.68eV, static refractive index $n(0)$ = 1.648 were reported in this study. To investigate on the electronic and elastic properties of W-ZnO, Gopal and Spaldin [32] used the VASP code to implement DFT with Self- Interaction Corrected [33] and LDA potentials for comparison. While the standard LDA underestimated the band gap at 0.78eV, SIC-LDA overestimated it at 3.8eV. The five independent elastic constants for hexagonal W-ZnO obtained with SIC-LDA potentials were C11=217, C12=117, C13=121, C33=225 and C44=50 GPa. From the above discussion, DFT has been verified as a reliable and effective computational technique in the study of fundamental material properties. However, the band gap underestimation in the standard DFT is a major limitation in the accurate prediction of electronic properties of materials. The use of approximated potentials in the Kohn-Sham implementation, results to generation of self-interaction errors [34,35]. The hybridization between the Zn-3d and O-2p shells is therefore inadequately dealt with by standard semi-local exchange correlation (XC) functionals, resulting into the shrinking of the band gap [36]. Several approaches have been proposed to compensate for the band gap underestimation of standard DFT formalism. Green functional (GW) approximation [37,38] puts into consideration the self-energy of a many-body system of electrons and has been used to reproduce the experimental band gaps of semiconductors. On the other hand, hybrid exchange-correlation functionals [39-41] like HSE, PBE0, and B3LYP integrates the GGA exchange potentials with the Hartree–Fock (HF) non-local exact exchange to widen the band gap. Although GW and hybrid potentials have proven to be more accurate than standard DFT, their high computational cost limits their applications. In the recent past, Tran and Blaha modified Becke-Johnson (TB-mBJ) potential have been developed to allow better approximations of band gaps at a reasonable computational cost [42,43]. DFT+U formalism proves to be the most popular remedy to DFT limitationsfor their ease of implementation, low computation cost and high accuracy. DFT+U introduces an on-site Coulombic Hubbard U term [44] into the XC functional of either the LDA or GGA. The magnitude of the on-site potential is basically defined by parameters U (on-site Coulomb) and J (on-site exchange), which can be obtained from first-principle calculations or by comparison with experimental data [45,46]. In the simplistic implementation of DFT+U proposed by [47], the Columbic interaction is included via an effective U_{eff} (= U−J) parameter as shown in equation (1).

$$E_{DFT+U} = E_{DFT} + \sum_a \frac{U_{eff}}{2} Tr\,(\rho^a - \rho^a \rho^a) \qquad (1)$$

Where ρ^a is the atomic orbital matrix. Generally, it is not easy to deduce the optimal value of the coulombic potential U for ZnO. This is after the widely used linear response approach provided by Cococcioni *et al.* [48] for open-shell systems failed on ZnO since it is a closed-shell system. Dependence of the band gap and lattice parameters of ZnO on the value of Hubbard U has been proposed as a viable route in the determination of the optimal value of U [49]. Huang *et al*. [50] compared the impact of the Hubbard U term on the structural and electronic aspects of W-ZnO using LDA+U and GGA+U approximation. They introduced the Hubbard U term on both the d orbital of Zn (U_d) as well as the p orbital of oxygen (U_p). This method resulted into improved band gap as well as the position of the valence band with GGA+U reporting an improvement of the energy band gap from 0.7 eV to 1.4 eV. Recently, Goh *et al*. [51] carried out a similar study by applying Hubbard corrections U_d to Zn- 3d states and U_p to O-2p states in the LDA+U method. According to this study, while the band gap was enlarged towards experimental value, the lattice constants were underestimated for all the tested Hubbard parameters. So far, the influence of U_d and U_p on W-ZnO has largely been focused on structural and electronic properties while their effect on mechanical and optical properties has been greatly ignored. To the best of our knowledge, there exists no report on the optical and mechanical properties of W-ZnO based on the DFT + U_d + U_p formalism. Whereas the mechanical properties determines the stability of a compound, optical properties such as dielectric functions, absorption, reflectivity, energy loss and refractive index describes the applicability of a compound in DSSCs. To explore the potential candidature of W-ZnO as a photoanode in DSSCs, this study adopted the DFT + U_d + U_p method to investigate the structural, mechanical, electronic and optical properties of W-ZnO.

2. Computational Details

Ab initio calculations were conducted utilizing the density functional theory (DFT) framework as implemented in the Quantum ESPRESSO (QE) software [52]. Self-consistent calculations were executed to address the Kohn-Sham equations [53] within the Generalized Gradient Approximation, employing the Perdew-Burke-Ernzerhof (GGA-PBE) [54] exchange-correlation functional. The W-ZnO compound exhibits a hexagonal structure that belongs to the P63mc

space group, characterized by angles α = β = 90° and γ = 120°, with lattice parameters a = b = 3.25 Å and c = 5.21 Å [17]. The unit cell of W-ZnO comprises four atoms, specifically two zinc (Zn) atoms and two oxygen (O) atoms. To ensure the precision of the results, structural optimization was performed. The convergence of k-points was assessed, ranging from 3 × 3 × 1 to 18 × 18 × 16, with increments of 2 × 2 × 2. Additionally, the kinetic energy cut-off (Ecut) was optimized within a range of 10 to 100 Ry, with steps of 5 Ry. Following this, lattice constant optimization was conducted utilizing the converged k-point and cut-off energy values, achieving convergence with a criterion set at 10^{-4} Ry. The K-point sampling of the Brillouin zone was implemented using the Monkhorst and Pack method, establishing a grid of 8 × 8 × 6 K-points. Electronic band structure calculations were performed employing both the Generalized Gradient Approximation (GGA) and GGA+U methodologies. This comparative analysis was necessary due to the tendency of Local Density Approximation (LDA) and GGA functionals to underestimate the electronic band gaps of materials. The THERMO-PW software was utilized to compute both the real and imaginary components of the dielectric function under standard DFT and DFT+U frameworks. Furthermore, THERMO-PW was also applied to evaluate the mechanical properties, with normal cell relaxation conducted to ensure a stress-free system prior to the calculation of elastic constants. Various elastic properties were derived using the Voigt (V), Reuss (R), and Hill (H) averaging methods. The bulk modulus, which serves as an indicator of incompressibility, was calculated as the average of Bv and B_R, as outlined in equations 2-4.

$$B_V = \frac{1}{9}[2(C_{11} + C_{12}) + C_{33} + 4C_{13}] \quad (2)$$

$$B_R = \frac{(C_{11}+C\_12)C_{33}-2C_{13}^2}{C_{11}+C_{12}+2C_{33}-4C_{13}} \quad (3)$$

$$B_H = \frac{B_V+B_R}{2} \quad (4)$$

The shear modulus describing a deformation caused by a stretching force acting parallel to an invariant line was computed using equations 5-7.

$$G_V = \frac{1}{30}(C_{11} + C_{12} + 2C_{33} - 4C_{13} + 12C_{44} + 12C_{66}) \quad (5)$$

$$G_R = \frac{5}{2}\frac{\{(C_{11}+C\_12)C_{33}-2C_{13}^2\}C_{44}C_{66}}{3B_VC_{44}C_{66}+\{(C_{11}+C_{12})C_{33}-2C_{13}^2\}(C_{44}+C_{66})} \quad (6)$$

$$G_H = \frac{G_V+G_R}{2} \quad (7)$$

To compute the young modulus (E), Poissons ratio (n) and Pugh ratio (P), Shear anisotropy (A) and Debye temperature, equations 8-12 were used.

$$E = \frac{9BG}{3B+G} \quad (8)$$

$$n = \frac{1}{2}\left\{1 - \frac{E}{3B}\right\} \quad (9)$$

$$P = \frac{B}{G} \quad (10)$$

$$A = \frac{2C_{44}}{C_{11}-C_{12}} \quad (11)$$

$$\Theta_D = \frac{\hbar}{k}\left[\frac{3n}{4\pi}\left(\frac{N_A\rho}{M}\right)\right]^{1/3} V_m \quad (12)$$

Where $\hbar$ represents Planck's constant, k denotes Boltzmann's constant, NA signifies Avogadro's number, n indicates the number of atoms per formula unit, M refers to the molecular mass per formula unit, ρ is the density, and Vm is derived from equation 13.

$$V_m = \left[\frac{1}{3}\left(\frac{2}{V_s^3+V_l^3}\right)\right]^{-1/3} \quad (13)$$

Where V_s and V_l are the shear and longitudinal sound velocities.

3. Results and Discussions

3.1. Structural Properties

The optimization of structural parameters is a significant part of theoretical understanding of a material [60]. Figure 1 illustrates the visual depiction of the hexagonal phase of ZnO that was examined in this research.

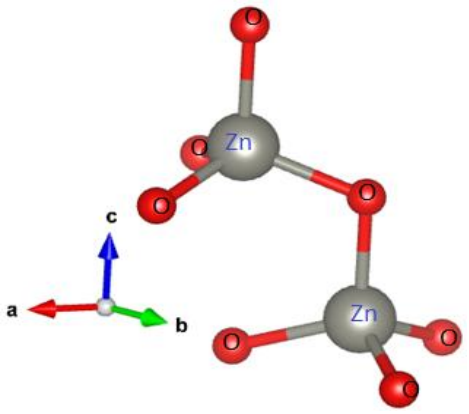

Figure 1. Schematic representation of hexagonal wurtzite structure of ZnO using VESTA code [61]

The W-ZnO crystal is characterized by the presence of two interpenetrating hexagonal close-packed (hcp) sub-lattices. Each sub-lattice is composed of a single type of atom that is offset relative to the other along the threefold c-axis, with an internal parameter u of 0.375, which is indicative of an ideal wurtzite structure [17]. In this structure, each zinc atom bonds with four oxygen atoms situated at the corners of a regular tetrahedron and vice versa as shown in Figure 1. For the accuracy and viability of any DFT study, the optimal values of k-points, kinetic energy cut off (Ecut) and lattice constants are very crucial. The ideal density of k-points is directly related to the volume of the compound, and due to zinc's classification as a transition metal, it necessitates a higher density of k-points. By varying the k–points grid over a wide range (3x3x1 to 18x18x16), the first Brillouin zone was integrated up to a minimum k-point mesh of 8x8x6 as shown in Figure 2 (a). To optimize the Ecut, the optimized k-point mesh and experimental lattice constants for W- ZnO were fixed while Ecut was varied from 10-100 Ry. The wave functions converged at 50Ry as shown

in Figure 2 (b) which was computationally cost effective.

The lattice parameters were optimized at fixed k-point and Ecut by varying lattice constant, a in the range of 3.19- 3.4Å and the ratio c/a in the range of 1.55-1.65 Å . Figure 3 (a), (b) and (c) presents optimized values of lattice constant a, c/a ratio and volume respectively. From these Figures, the optimal lattice constants $a = b = 3.289$ Å and $c = 5.29032$ Å were obtained. This yielded a *c/a* ratio of 1.608, which is close to the experimental value of 1.60 expected for hcp unit cells [17]. The optimal cell volume achieved was 49.39 $Å^3$ which is in good agreement with the experimental value of 48.15 $Å^3$ [17] and DFT value of 45.67 [62] implying that our technique is viable and the obtained findings are reliable. The introduction of Hubbard U potential has a reducing effect on the lattice constants and volume as shown in Figure 3 (a), (b) and (c). This is attributed to the decreased hybridization of Zn-3d and O-2p orbitals with the inclusion of the Hubbard U term [44].

Table 1. Optimized lattice constants a, c/a, equilibrium volume (V_0), bond length, bond angle and minimum energy (E_{min})

	a (Å)	c/a	V_0(Å ^{3})	Bond length (Å)	Bond angle	E_{min}(Ry)
DFT	3.289	1.608	49.39	1.9993	108.37	-570.91
DFT+ U_d	3.276	1.603	49.26	1.9982	108.41	-570.45
DFT+U_d + U_p	3.269	1.594	48.84	1.9975	108.45	-570.31
Experiment	3.264 [17]	1.599 [17]	48.15 [17]	1.992 [17]	-	-
Other DFT work	3.20 [62]	1.609 [62]	45.67 [62]	1.98[63]	-	-

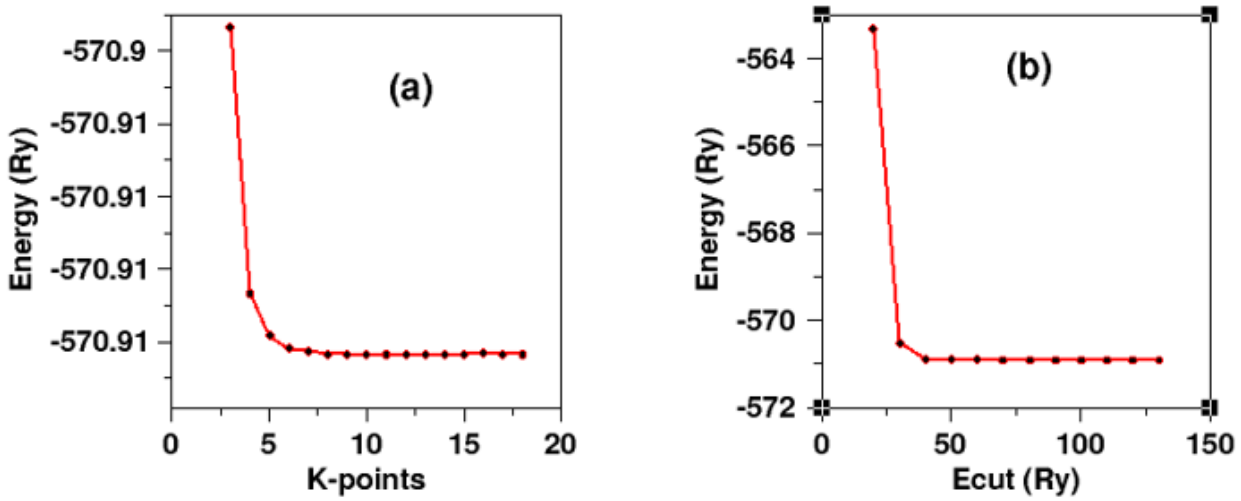

Figure 2. Total energies of W-ZnO as a function of (a) k-point mesh (b) cut-off energy

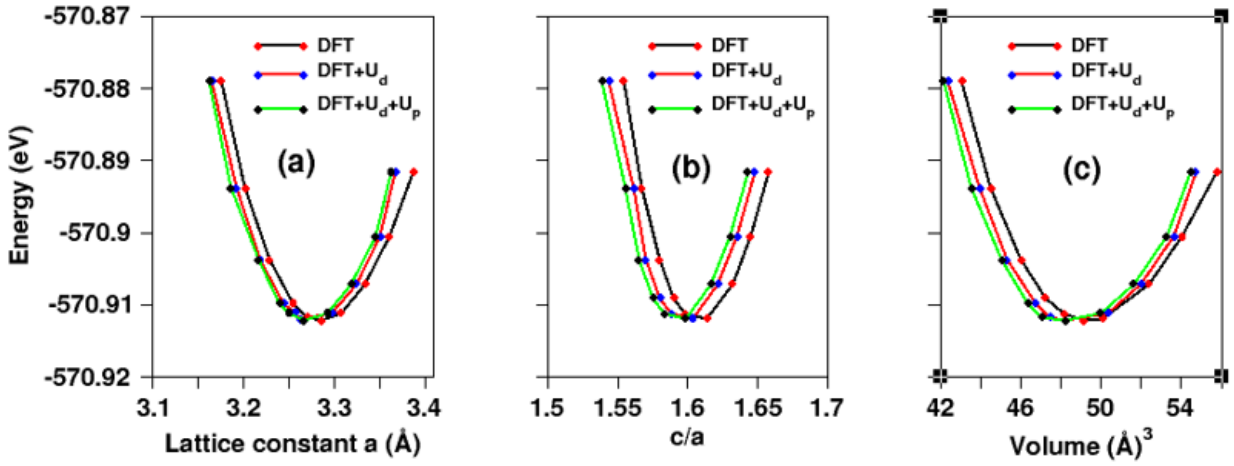

Figure 3. Total energies of W-ZnO as a function of (a) lattice constant (b) c/a and (c) volume

While bond length is the average distance between the nucleus, bond angle describes the angle between two atomic bonds. In this study, the bond length and bond angles of W-ZnO were determined using Xcrysden code. The impact of introducing the Hubbard U term on bond length and bond angle were investigated and the results presented in Table 1. The shortening of the bond length with the inclusion of Hubbard U is attributed to the reduction of lattice constants in the DFT+U calculations as discussed earlier in this paper.

3.2. Mechanical Properties

The elastic constants, C_{ij}, are critical distinctives for interpretation of the mechanical performance of stressed materials. The constants provide insights into the interactions between neighboring atomic planes, as well as the anisotropic characteristics of binding, stiffness, and structural integrity. W-ZnO exhibits a hexagonal crystal structure, which is characterized by six elastic constants: C_{11}, C_{12}, C_{13}, C_{33}, C_{44}, and C_{66}. While the first five constants are independent of one another, the sixth constant is determined as a function of the first two, as outlined in equation 14 [64].

$$C_{66} = \frac{1}{2}(C_{11} - C_{12}) \tag{14}$$

Table 2. Calculated elastic constants (c_{ij}) for W-ZnO

	C_{11}	C_{12}	C_{13}	C_{33}	C_{44}	C_{66}
DFT	195.3	98.31	99.47	192.2	37.4	48.5
DFT+U	195.4	104.3	110.2	190	36.4	45.6
LDA ref [65]	227	133	118	232	40	47
Expt ref [66]	206	110	118	211	44.3	44.6

The calculated elastic constants are presented in Table 2 for both DFT ad DFT+U frameworks and we obtain overall good agreement with experimental and other DFT findings.

For hexagonal system to be declared mechanically stable, the elastic constants need to obey stability criteria described by equations 15-20 [64].

$$C_{11} > 0 \tag{15}$$

$$C_{33} > 0 \tag{16}$$

$$C_{44} > 0 \tag{17}$$

$$C_{11} > |C_{12}| \tag{18}$$

$$C_{11}^2 > C_{12}^2 \tag{19}$$

$$(C_{11} + 2C_{12})\, C_{33} > 2C_{13}^2 \tag{20}$$

From the results of Table 2, the elastic constants fulfill all the above conditions, confirming the mechanical stability of W-ZnO. The elastic constants C_{11} and C_{33} denote the resistance to linear compression in the a and c orientations, respectively. The magnitudes of C_{11} and C_{33} are significantly greater than those of other elastic constants, indicating that ZnO exhibits incompressibility in both the a and c directions when exposed to stress. Furthermore, the greater value of the elastic constant C_{11} in comparison to C_{33} suggests that the incompressibility in the a-direction is more pronounced than that in the c-direction. By use of equations 9-20, other fundamental elastic characteristics including the young modulus (E), Poissons' ratio(n) and Pugh ratio (P), Shear anisotropy (A) and Debye temperature, were calculated and presented in Table 3.

Table 3. Elastic moduli, Poisson's ratio (n), Pugh's ratio (B/G), shear anisotropy, Debye Temperature and shear velocity of ZnO in comparison with other previous studies

	B (GPa)	E (GPa)	G (GPa)	Poissons Ratio	Pugh Ratio (B/G)	Shear Anisotropy (A)	Debye Temp (K)	Shear Velocity (m/s)
DFT	136.9	113.4	41.8	0.36	3.28	0.77	414.84	3218.95
DFT+U	136.7	107.2	39.1	0.37	3.50	0.799	463.99	3600
LDA ref [60]	162		-	-	-	-	-	-
Expt ref [61]	142.4	-	-	-	-	-	-	-

From the value of bulk modulus obtained, W-ZnO reveals itself as an incompressible compound with a high bond strength. The computational findings corroborate with previous experimental and DFT studies as indicated in Table 3. Additionally, good agreement is observed on the findings of bulk modulus (136.8 GPa) computed by fitting equilibrium volume in the Murnaghan equation of state (MEoS) [67] described by equation (21).

$$E(V) = \frac{B_o V}{B_0^1}\left[\left(\frac{V_0}{V}\right)^{B_0^1}\frac{1}{B_0^1 - 1} + 1\right] + const \tag{21}$$

The shear modulus quantifies the hardness of a material. The computed values of shear modulus 41.8 and 39.1 GPa in the DFT and DFT+U calculations respectively are good indicators of the hardness of W-ZnO. Larger stiffness is predicted by DFT than DFT+U since the observed young's modulus of 113 GPa in standard DFT is larger than 107.2 GPa obtained in DFT+U. Bulk Modulus (B) and Shear modulus (G) are utilized in computing the Pugh's ratio (B/G), which is a measure of theductility of a materials. B/G >1.75, indicates ductility, whereas B/G <1.75 suggests brittleness of a material. For ZnO, the B/G ratios are 3.28 and 3.50in the DFT and DFT+U respectively, implying that this material is highly ductile. The poison's ratio (n) serves as a critical parameter in assessing material properties; specifically, a value greater than 0.26 indicates ductility, whereas a value less than 0.26 signifies brittleness. The calculated values of n are 0.36 and 0.37 in the DFT and

DFT+U calculations respectively confirming the ductility of ZnO. Debye's temperature indicates the temperature necessary for the activation of all the crystal's phonon modes in a material. The high Debye's temperature of 414.84 and 463.99 K obtained in this study for DFT and DFT+U computations respectively indicate high thermal conductivity of ZnO. For isotropic crystals systems, the value of shear anisotropies (A) is expected to be equal to 1. The shear anisotropy of a crystal is determined by values that are either below or above 1. Since we obtained an A of 0.77 and 0.799 for DFT and DFT+U techniques respectively, ZnO can therefore be said to be purely anisotropic. Shear velocity is another fundamental parameter that describes the lattice's thermal conductivity. From this study, although, DFT+U calculation predicted a higher shear velocity (3600m/s) for W-ZnO as compared to DFT (3218.95 m/s), both formalism suggests a high thermal conductivity of W-ZnO.

3.3. Electronic Properties

The electronic characteristics were examined through the computation of electronic band structures and the associated projected density of states (PDOS), as illustrated in Figures 5, 6, and 7. The dashed lines at 0 eV in these figures indicate the Fermi energy level, which delineates the boundary between the conduction band and the valence band. To enhance the accuracy of the electronic band structure calculations, the K point mesh was refined to a denser configuration by sampling the high symmetry points within the first Brillouin zone. In this research, the band structures are illustrated at the high symmetry points Ao-Eo– Γ-S-Y- Z. Analysis of these band structures reveals that both the valence band maxima (VBM) and the conduction band minima (CBM) are located at the gamma symmetry point. As a result, W-ZnO exhibits a direct band gap of 0.79 eV when evaluated using the standard DFT formalism. This is a great improvement from the QE the value of 0.65 eV reported by Qing *et al* [28]. In contrast to the experimentally determined band gap of 3.37 eV, it is an extreme underestimation of approximately 75%. The observed phenomenon can be ascribed to the recognized limitations of Local Density Approximation (LDA) and Generalized Gradient Approximation (GGA) in addressing the significant hybridization between the d and p orbitals, which results in a reduction of the band gap. [68]. Introduction of the Hubbard correction term in the Zn-3d (U_d) and O-2P (U_p) shells significantly widened the band gap. Figure 4(a) and (b) presents the band gap variation with Hubbard U values exhibiting a direct correlation obtained in both DFT + U_d and DFT + U_d + U_P calculations. A combination of U_d =10 eV and Up= 8 eV reproduced experimental band gap of 3.19eV as reported by [17] and was therefore adopted in consequent computations of the optical and mechanical properties.

These energy band gaps corroborates with the findings of the PDOS presented in Figures 5b, 6b and 7b. From the PDOS calculations, VB is primarily dominated by the O-2s, Zn-3d and O-2P orbitals. On the other hand, the Zn-4s and O-2P contributes in to the conduction band. The contribution of Zn-2s and Zn-2p is not well pronounced in both the VB and CB. The incorporation of the Hubbard term U results in a downward shift of the hybridized Zn-3d and O-2p states, while the Zn-4s state experiences an upward shift. As a result, the band gap is increased, and the Fermi level moves closer to the valence band.

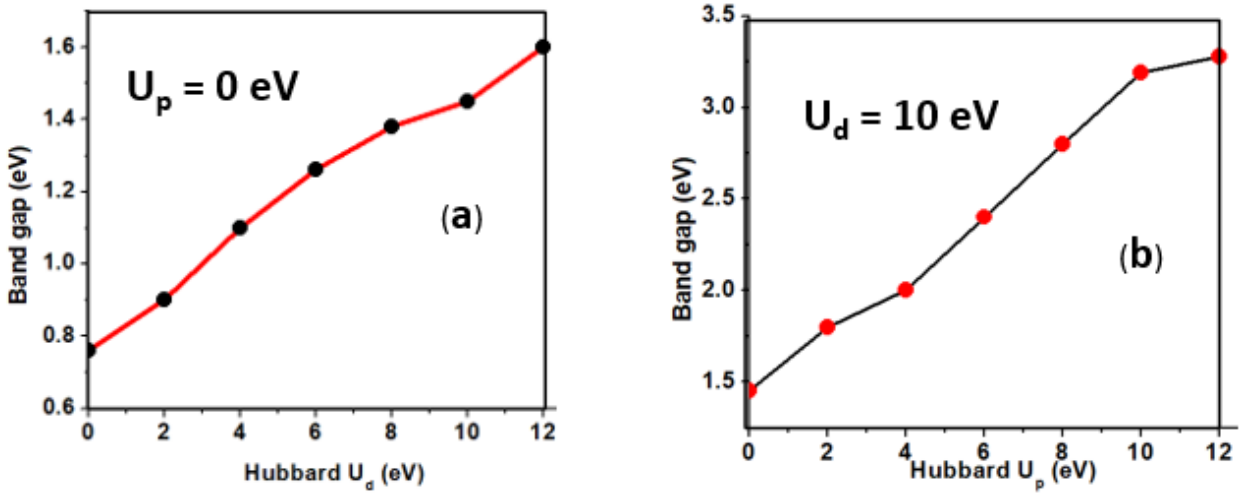

Figure 4. The variation of the Hubbard U parameter and the band gap. (a) DFT + U_d and (b) DFT+U_d +U_p

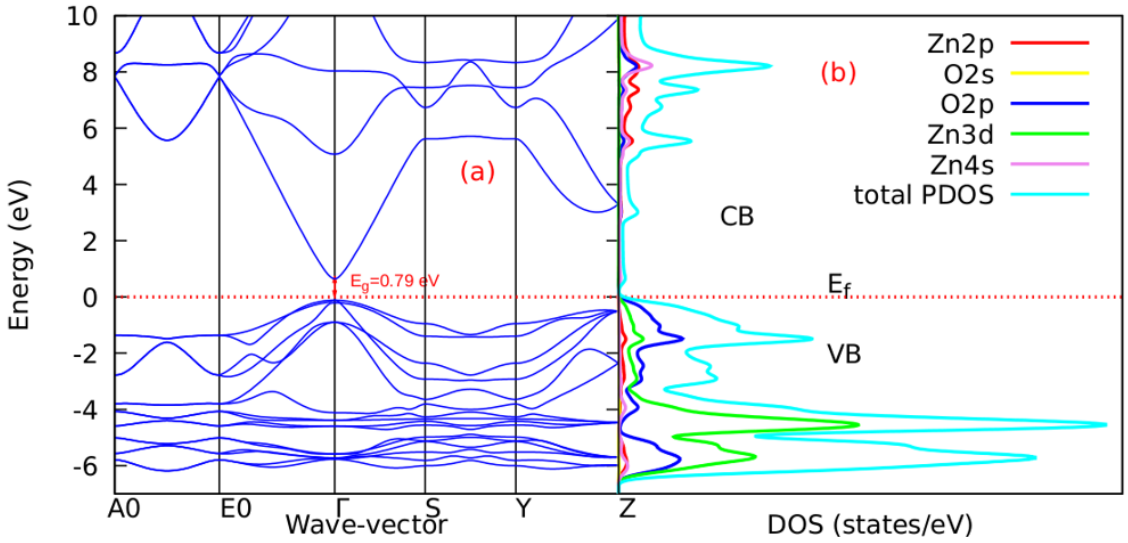

Figure 5. Band structure and density of state of W-ZnO using standard DFT approximation

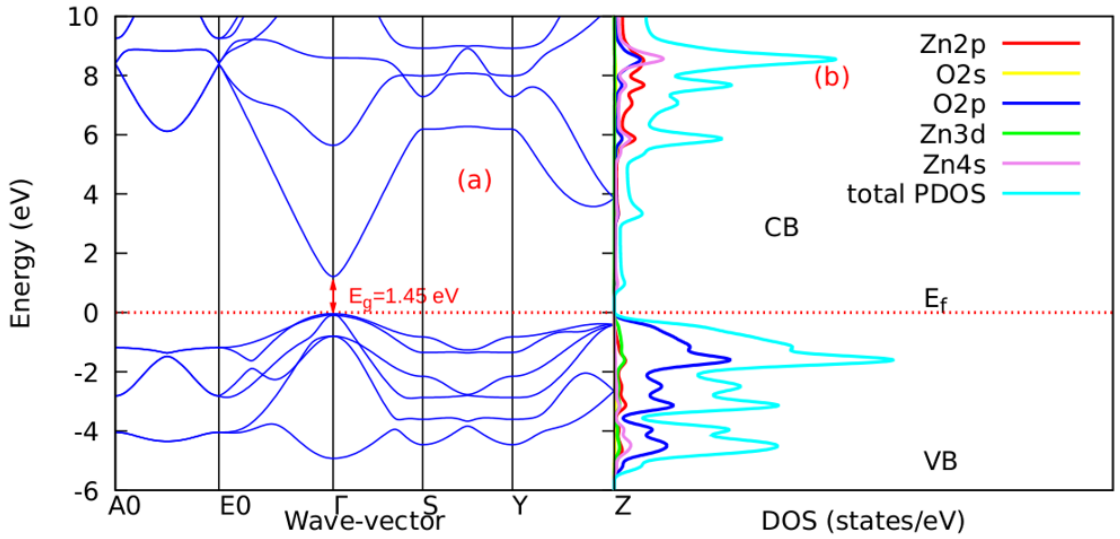

Figure 6. Band structure and density of state of W-ZnO using DFT+$U_{d(10eV)}$ approximation

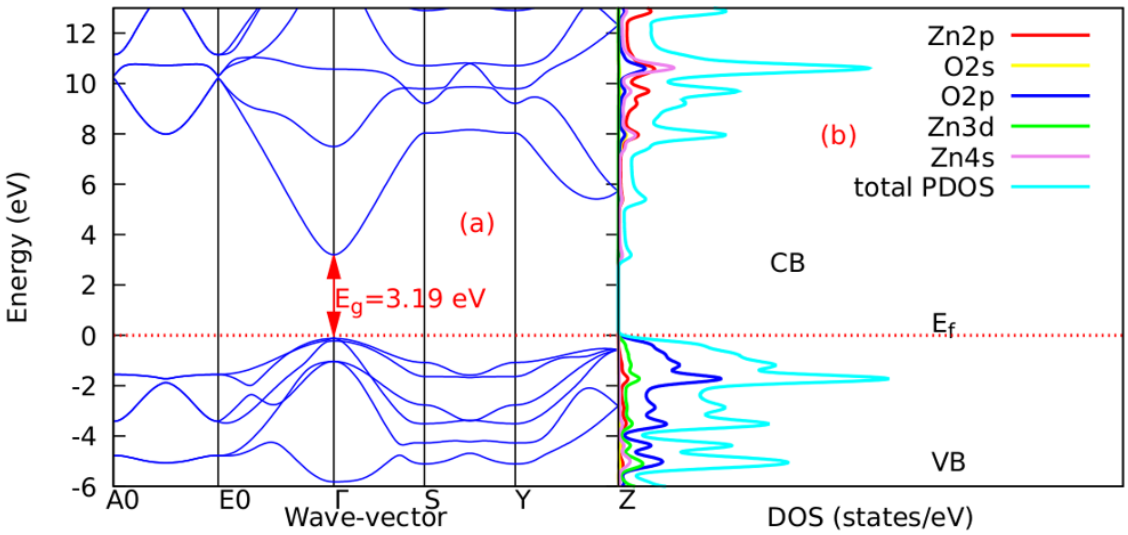

Figure 7. Band structure and density of state of ZnO using DFT + $U_{d(10eV)}$+ $U_{p(8eV)}$ approximation

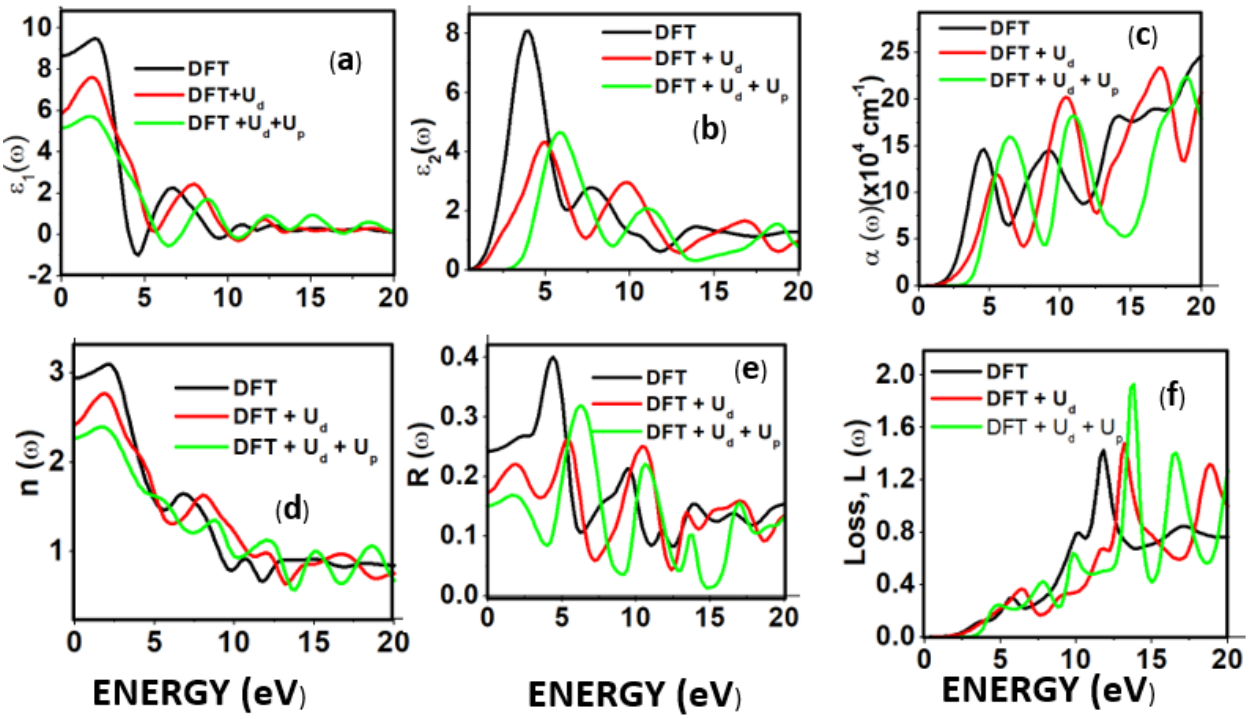

Figure 8. The (a) real (b) imaginary part of the dielectric constant, (c) absorption coefficient, (d)refractive index, (e) reflectivity and (f) energy loss as a function of the energy in eV of ZnO using DFT, DFT + U_d and DFT+U_d +U_p

3.4. Optical Properties

An appropriate compound for utilization in the photoanode of a dye-sensitized solar cell (DSSC) must be selected based on its optical characteristics. The optical properties of a material elucidate the frequency-dependent response of various optical parameters to the energy of incoming photons, represented by the equation E = hv. The optical parameters of a material are characterized by ε(ω), a complex dielectric function that varies with frequency. The expression for ε(ω) is detailed in relation (22) [69].

$$\varepsilon(\omega) = \varepsilon_1(\omega) + i\varepsilon_2(\omega) \quad (22)$$

Where $\varepsilon_1(\omega)$ and $\varepsilon_2(\omega)$ represent the real and imaginary components, respectively, of the complex dielectric function. The real component elucidates the dispersion of photons and the degree of polarization within the material, whereas the imaginary component accounts for the absorption of photons by the material. According to the selection rules, the calculations of the momentum matrix elements between unoccupied and occupied wave functions, as outlined in equation 23, yield the imaginary part $\varepsilon_2(\omega)$ (70)

$$\varepsilon_2(\omega) = \frac{8\pi^2 e^2}{\omega^2 m^2}$$

$$\sum_n \sum_{n'} \int |P^v_{nn'}(k)|^2 f_{kn}(1 - f_{nn'})\delta\left(E^k_n - E^k_{n'} - \hbar\omega\right)\frac{d^3k}{(2\pi)^3} \quad (23)$$

The real part $\varepsilon_1(\omega)$ is derived from $\varepsilon_2(\omega)$ using the Kramer – Kronig relationbelow [71]

$$\varepsilon_1(\omega) = 1 + \frac{2}{\pi}\int_0^\infty \frac{\varepsilon_2(\omega)\omega' d\omega'}{\omega'^2 - \omega^2} \quad (24)$$

The extraction of other optical constants, including the absorption coefficient α(ω), refractive index n(ω), energy loss spectrum L(ω), and reflectivity R(ω), was conducted using $\varepsilon_1(\omega)$ and $\varepsilon_2(\omega)$ as described in equations 25-28.

$$\alpha(\omega) = \sqrt{2\omega}\left(\sqrt{\varepsilon_1^2(\omega) + \varepsilon_2^2(\omega)} - \varepsilon_1(\omega)\right)^{\frac{1}{2}} \quad (25)$$

$$n(\omega) = \frac{1}{\sqrt{2}}\left(\frac{\sqrt{\varepsilon_1^2(\omega)+\varepsilon_2^2(\omega)}+\varepsilon_1(\omega)}{2}\right)^{\frac{1}{2}} \quad (26)$$

$$L(\omega) = \frac{\varepsilon_2(\omega)}{\varepsilon_1^2(\omega)+\varepsilon_2^2(\omega)} \quad (27)$$

$$R(\omega) = \frac{(n-1)^2+K^2}{(n+1)^2+K^2} \quad (28)$$

The graphs depicted in Figure 8(a–f) display the relationship between optical properties and energy in eV. In reference to Figure 8(a), the electronic portion of the static dielectric function, is 8.52, 6.02 and 5.16 for DFT, DFT + U_d and DFT+U_d +U_p calculations respectively. The calculation of refractive indices is achieved by taking the square roots of the specified values [34], which are summarized in Table 4. From this table, the inclusion of Hubbard U term reduces the value of $\varepsilon_1(0)$ as well as the refractive index. Between 5.1 to 5.8 eV, the curve is negative implying that the radiation is at this point fully attenuated and the ZnO compound behaves like a metal [71]. The imaginary spectrum provides a connection between the optical and electronic band structure of a material. From figure 8(b) of $\varepsilon_2(\omega)$ as a function of energy, the critical onset points are located at 0.78, 1.46and 3.19 eV for DFT, DFT + U_d and DFT+U_d +U_p calculations

respectively as tabulated in Table 4. The increase in the critical point value from DFT to DFT + U_d to DFT+U_d +U_p is collaborative to the results of computed electronic band gaps. The $\varepsilon_2(\omega)$ plot exhibited three prominent peaks at energies of 5.12, 10.4, and 13.6 eV, which correspond to the transition of an electron from the valence band to the conduction band. In this context, the transitions of electrons occur between the O-2p and Zn-4s orbitals, the O-2p and Zn-3d orbitals, as well as between the O-2s and Zn-3d orbitals, respectively. The absorption coefficient describes how light intensity diminishes over a specified distance within a material medium. It is greatly affected by the photon frequency implying that the incident photon interacts with material electrons resulting in interband electron transition from the valence to conduction bands. The data presented in Figure 8(c) indicates that the absorption edge of W-ZnO occurs at 0.78 eV, 1.44 eV, and 3.19 eV, corresponding to the DFT, DFT + U_d, and DFT + U_d + Up calculations, respectively. Contrast to standard DFT which predicts absorption of low energy photon including infrared, the DFT+U_d +U_p approach reveals that ZnO is transparent to majority of the solar radiation. Consequently, ZnO is able to pass on light to the absorption dye for photoemission and hence current generation [71]. The refractive index, a dimensionless parameter of an optical medium, quantifies the degree to which a light beam is bent when traversing through that medium. [72]. Materials of considerably high (above 1.8) refractive index are desired in photovoltaic applications. The calculated refractive index of W-ZnO is displayed in the plot of Figure 8(d) and the results are presented in Table 4. Despite the reduction of static refractive indices from DFT to DFT + U_d to DFT+U_d +U_p, the values are high enough for the application of ZnO as a DSSC photoanode. A substantial drop in the dispersion curve related to the refractive index was observed post the initial peak indicating that beyond a certain amount of photon energy, W-ZnO fails to maintain its transparent nature and instead absorbs such radiations.

Reflectivity depicts the surface behavior of a material. Figure 8(e) shows a low reflectivity at zero photon energy (R_0). From Table 4, DFT+U_d +U_p predicts the least reflectivity of W-ZnO implying the ability of this material to reflect minimum solar radiation but instead allow it to pass through for dye excitation in DSSC. From the plot, the highest peaks are observed at approximately 4.9, 5.1 and 5.8 eV in the DFT, DFT + U_d and DFT+U_d +U_p respectively after which the reflectivity rapidly dropped. Energy lossL (ω) is another vital parameter that characterizes the loss of energy of a fast-moving electron as it transverses a material medium. Figure 8(f) shows a near zero energy loss up to 4.0 eV all the approximations techniques. At higher photon energy, the energy loss in ZnO gradually rises to a peak at 12.8, 14.2 and 15.4 eV DFT, DFT + U_d and DFT+U_d +U_p respectively. The capability of W-ZnO within UV-Vis region to retain most of its energy with negligible energy loss to the surrounding as desired in DSSCs photoanode is therefore confirmed. However, for high-energy electrons, the energy loss of W-ZnO is relatively high.

Table 4. Real dielectric function at 0 eV{$\varepsilon_1(0)$}, refractive index (n), absorption critical points and reflectivity at 0 eV (R_0)

	$\varepsilon_1(0)$	Refractive index	Absorption critical points	R(0)
DFT	8.52	2.92	0.78	0.24
DFT + U_d	6.02	2.45	1.44	0.15
DFT+U_d +U_p	5.16	2.27	3.19	0.09

4. Conclusions

In this ab initio study, the potentiality and stability of W-ZnO as a potential photoanode in DSSCs has been investigated. The material was observed to exhibit hexagonal crystalline structure with lattice constant a=b= 3.289Å and c=5.29Å . Upon inclusion of Hubbard U, the lattice constants decreased with increase in both U_d and Up. Direct band gap of 0.79, 1.45 and 3.19 eV were obtained for DFT, DFT + Ud(10eV) and DFT+Ud(10ev) + Up(8eV) respectively. This showed that the Hubbard U term has a positive effect on the accuracy of band gap approximation. The inclusion of Hubbard potential in the O-2p is a noble technique that can be utilized even in other metal oxide material to enhance DFT accuracy at no extra computational cost. The computed elastic constants adhered to the stability criteria for hexagonal structures, thereby affirming the mechanical stability of W-ZnO. Optical absorption onsets were realized at 0.78 eV, 1.44 eV and 3.19 eV in DFT, DFT + Ud and DFT+Ud +Up calculations respectively. This reflects the energy band gap characteristic of ZnO which demonstrates W-ZnO as a transparent material in infra-red and visible light regions and only starts to absorb at UV region. W-ZnO has minimal energy loss in the solar radiation spectrum and hence light can easily transverse its structure. The properties examined in this study establishes the applicability of W-ZnO as a DSSC photoanode.

Declaration of Competing Interest

The authors indicate that there are no known financial conflicts or personal relationships that may have had an apparent effect on the work detailed in this paper.

Data Availability

Data can be provided upon inquiry.

ACKNOWLEDGEMENTS

The author expresses sincere gratitude to the Centre of High-Performance Computing (CHPC) located in Cape Town, South Africa, for their provision of the computational resources utilized in this research, specifically through the project MATS1181.

REFERENCES

[1] Grätzel M. And O'Regan B. (1991). A low-cost, high-efficiency solar cell based on dye-sensitized colloidal TiO_2 films, *Nature*, 353:737–740.

[2] Duong, T. T., Choi, H. J., He, Q. J., Le, A. T., & Yoon, S. G. (2013). Enhancing the efficiency of dye sensitized solar cells with a SnO_2 blocking layer grown by nanocluster deposition. *Journal of Alloys and Compounds*, *561*, 206-210.

[3] Xu, F., Zhang, X., Wu, Y., Wu, D., Gao, Z., & Jiang, K. (2013). Facile synthesis of TiO_2 hierarchical microspheres assembled by ultrathin nanosheets for dye-sensitized solar cells. *Journal of Alloys and Compounds*, *574*, 227-232.

[4] Govindaraj R., Senthil M., Ramasamy P. and Mukhopadhyay S. (2014). Synthesis oftitanium dioxide nanostructures and their effects on current-voltage (I-V) performance in dye sensitized solar cells, *International Journal of Chem Tech Research,* 6: 5220-5225.

[5] Grätzel, M. (2003). Dye-sensitized solar cells. *Journal of photochemistry and photobiology C: Photochemistry Reviews*, *4*(2), 145-153.

[6] Huang, J., Yin, Z., & Zheng, Q. (2011). Applications of ZnO in organic and hybrid solar cells. *Energy & Environmental Science*, *4*(10), 3861-3877.

[7] Beek, W. J., Wienk, M. M., & Janssen, R. A. (2006). Hybrid solar cells from regioregularpolythiophene and ZnO nanoparticles. *Advanced Functional Materials*, *16*(8), 1112-1116.

[8] Zhang, Q., Dandeneau, C. S., Zhou, X., & Cao, G. (2009). ZnO nanostructures for dye-sensitized solar cells. *Advanced materials*, *21*(41), 4087-4108.

[9] Lin, C. Y., Lai, Y. H., Chen, H. W., Chen, J. G., Kung, C. W., Vittal, R., & Ho, K. C. Energy Environ. Sci. 4, 3448 (2011).

[10] Lai, T. H., Tsang, S. W., Manders, J. R., Chen, S., & So, F. (2013). Properties of interlayer for organic photovoltaics. *Materials Today*, *16*(11), 424-432.

[11] M.Tan, M. J., Zhong, S., Li, J., Chen, Z., & Chen, W. (2013). Air-stable efficient inverted polymer solar cells using solution-processed nanocrystalline ZnO interfacial layer. *ACS applied materials & interfaces*, *5*(11), 4696-4701.

[12] Look, D. C., Reynolds, D. C., Sizelove, J. R., Jones, R. L., Litton, C. W., Cantwell, G., &Harsch, W. C. (1998). Electrical properties of bulk ZnO. *Solid state communications*, *105*(6), 399-401.

[13] Forro, L., Chauvet, O., Emin, D., Zuppiroli, L., Berger, H., & Levy, F. (1994). High mobility n-type charge carriers in large single crystals of anatase (TiO2). *Journal of Applied Physics*, *75*(1), 633-635.

[14] Wang, Z. L. (2004). Nanostructures of zinc oxide. *Materials today*, *7*(6), 26-33.

[15] Klingshirn, C. (2007). ZnO: material, physics and applications. *ChemPhysChem*, *8*(6), 782-803.

[16] Tributsch, H., & Calvin, M. (1971). Electrochemistry of excited molecules: photo-electrochemical reactions of chlorophylls. *Photochemistry and Photobiology*, *14*(2), 95-112.

[17] Ungula, J. (2015). *Growth and characterization of ZnO nanoparticles by sol-gel process* (Doctoral dissertation, University of the Free State (Qwaqwa Campus)).

[18] Ungula, J., Dejene, B. F., & Swart, H. C. (2018). Band gap engineering, enhanced morphology and photoluminescence of un-doped, Ga and/or Al-doped ZnO nanoparticles by reflux precipitation method. *Journal of Luminescence*, *195*, 54-60.

[19] Mahmoud, W. E. (2010). Synthesis and optical properties of Ce-doped ZnO hexagonal nanoplatelets. *Journal of crystal growth*, *312*(21), 3075-3079.

[20] Dhamodharan, P., Manoharan, C., Bououdina, M., Venkadachalapathy, R., & Ramalingam, S. (2017). Al-doped ZnO thin films grown onto ITO substrates as photoanode in dye sensitized solar cell. *Solar Energy*, *141*, 127-144.

[21] Kumar, V., Pandey, A., Swami, S. K., Ntwaeaborwa, O. M., Swart, H. C., & Dutta, V. (2018). Synthesis and characterization of Er3+-Yb3+ doped ZnO upconversion nanoparticles for solar cell application. *Journal of Alloys and Compounds*, *766*, 429-435.

[22] Finocchi, F. (2011). Density Functional Theory for Beginners: Basic Principles and Practical Approaches. *Institut des NanoSciences de Paris (INSP) CNRS and University Pierre et Marie Curie, Paris*.

[23] Zhang, X. J., Mi, W. B., Wang, X. C., & Bai, H. L. (2014). First-principles prediction of electronic structure and magnetic ordering of rare-earth metals doped ZnO. *Journal of alloys and compounds*, *617*, 828-833.

[24] Khuili, M., Fazouan, N., Abou El Makarim, H., El Halani, G., &Atmani, E. H. (2016). Comparative first principles study of ZnO doped with group III elements. *Journal of Alloys and Compounds*, *688*, 368-375.

[25] Haq, B. U., Ahmed, R., &Goumri-Said, S. (2014). DFT characterization of cadmium doped zinc oxide for photovoltaic and solar cell applications. *Solar energy materials and solar cells*, *130*, 6-14.

[26] Ozugurlu, E. (2021). Cd-doped ZnO nanoparticles: an experimental and first-principles DFT studies. *Journal of Alloys and Compounds*, *861*, 158620.

[27] Lee, Y. S., Peng, Y. C., Lu, J. H., Zhu, Y. R., & Wu, H. C. (2014). Electronic and optical properties of Ga-doped ZnO. *Thin Solid Films*, *570*, 464-470.

[28] Qing, X., Zhang, C., Gong, J., & Chen, S. (2021). Ab initio study of photoelectric properties in ZnO transparent conductive oxide. *Vacuum*, *191*, 110391.

[29] Khuili, M., Fazouan, N., Abou El Makarim, H., Atmani, E. H., Rai, D. P., & Houmad, M. (2020). First-principles calculations of rare earth (RE= Tm, Yb, Ce) doped ZnO: Structural, optoelectronic, magnetic, and electrical properties. *Vacuum*, *181*, 109603.

[30] Lei, X., Zhao, G. J., Liang, X. X., & Song, T. L. (2015 January). First-principle Studies of Lattice and Electronic Structure of BexZn1-xO. In *Journal of Physics: Conference Series* (Vol. 574, No. 1, p. 012049). IOP Publishing.

[31] John, R., & Padmavathi, S. (2016). Ab initio calculations on structural, electronic and optical properties of ZnO in wurtzite

phase. *Crystal structure theory and applications*, *5*(02), 24.

[32] Gopal, P., &Spaldin, N. A. (2006). Polarization, piezoelectric constants, and elastic constants of ZnO, MgO, and CdO. *Journal of Electronic Materials*, *35*(4), 538-542.

[33] J.P. Perdew, A. Zunger, Self-interaction correction to density-functional approximations for many-electron systems, Phys. Rev. B. 23 (1981) 5048–5079.

[34] Namisi, M. M., Musembi, R. J., Mulwa, W. M., &Aduda, B. O. (2023). DFT study of cubic, tetragonal and trigonal structures of KGeCl3 perovskites for photovoltaic applications. *Computational Condensed Matter*, *34*, e00772.

[35] Allan, L., Mulwa, W. M., Musembi, R. J., &Aduda, B. O. (2022). First Principles Study of the Structural, Mechanical, Electronic, and Lattice Dynamical Properties of the Half-Heusler Alloys ZrCoY (Y= Sb, Bi). *arXiv preprint arXiv:2204.03759*.

[36] Agapito, L. A., Curtarolo, S., & Nardelli, M. B. (2015). Reformulation of DFT+ U as a pseudohybridhubbard density functional for accelerated materials discovery. *Physical Review X*, *5*(1), 011006.

[37] Friedrich, C., Müller, M. C., & Blügel, S. (2011). Band convergence and linearization error correction of all-electron GW calculations: The extreme case of zinc oxide. *Physical Review B*, *83*(8), 081101.

[38] Zhang, M., Ono, S., Nagatsuka, N., & Ohno, K. (2016). All-electron mixed basis G W calculations of TiO 2 and ZnO crystals. *Physical Review B*, *93*(15), 155116.

[39] Uddin, J., &Scuseria, G. E. (2006). Theoretical study of ZnO phases using a screened hybrid density functional. *Physical Review B*, *74*(24), 245115.

[40] Gerosa, M. (2018). Special issue on self-interaction corrected functionals for solids and surfaces. *Journal of Physics: Condensed Matter*, *30*(23), 230301.

[41] Clark, S. J., Robertson, J., Lany, S., &Zunger, A. (2010). Intrinsic defects in ZnO calculated by screened exchange and hybrid density functionals. *Physical Review B*, *81*(11), 115311.

[42] Tran, F., & Blaha, P. (2009). Accurate band gaps of semiconductors and insulators with a semilocal exchange-correlation potential. *Physical review letters*, *102*(22), 226401.

[43] Khuili, M., El Hallani, G., Fazouan, N., Abou El Makarim, H., &Atmani, E. H. (2019). First-principles calculation of (Al, Ga) co-doped ZnO. *Computational Condensed Matter*, *21*, e00426.

[44] Mulwa, W. M., Ouma, C. N., Onani, M. O., & Dejene, F. B. (2016). Energetic, electronic and optical properties of lanthanide doped TiO2: An ab initio LDA+ U study. *Journal of Solid State Chemistry*, *237*, 129-137.

[45] Deng, X. Y., Liu, G. H., Jing, X. P., & Tian, G. S. (2014). On-site correlation of p-electron in d10 semiconductor zinc oxide. *International Journal of Quantum Chemistry*, *114*(7), 468-472.

[46] Harun, K., Salleh, N. A., Deghfel, B., Yaakob, M. K., & Mohamad, A. A. (2020). DFT+ U calculations for electronic, structural, and optical properties of ZnO wurtzite structure: A review. *Results in Physics*, *16*, 102829.

[47] S.L. Dudarev, G.A. Botton, S.Y. Savrasov, C.J. Humphreys, A.P. Sutton, Electron-energy-loss spectra and the structural stability of nickel oxide: An LSDA+U study, Phys. Rev. B. 57 (1998) 1505–1509.

[48] Cococcioni, M., & De Gironcoli, S. (2005). Linear response approach to the calculation of the effective interaction parameters in the LDA+ U method. *Physical Review B*, *71*(3), 035105.

[49] Ma, X., Wu, Y., Lv, Y., & Zhu, Y. (2013). Correlation effects on lattice relaxation and electronic structure of ZnO within the GGA+ U formalism. *The Journal of Physical Chemistry C*, *117*(49), 26029-26039.

[50] Huang, G. Y., Wang, C. Y., & Wang, J. T. (2012). Detailed check of the LDA+ U and GGA+ U corrected method for defect calculations in wurtzite ZnO. *Computer Physics Communications*, *183*(8), 1749-1752.

[51] Goh, E. S., Mah, J. W., & Yoon, T. L. (2017). Effects of Hubbard term correction on the structural parameters and electronic properties of wurtzite ZnO. *Computational Materials Science*, *138*, 111-116.

[52] Giannozzi, P., Baroni, S., Bonini, N., Calandra, M., Car, R., Cavazzoni, C., &Wentzcovitch, R. M. (2009). QUANTUM ESPRESSO: a modular and open-source software project for quantum simulations of materials. *Journal of physics: Condensed matter*, *21*(39), 395502.

[53] Kohn, W., & Sham, L. J. (1965). Self-consistent equations including exchange and correlation effects. *Physical review*, *140*(4A), A1133.

[54] Perdew, J. P., Burke, K., & Ernzerhof, M. (1996). Generalized gradient approximation made simple. *Physical review letters*, *77*(18), 3865.

[55] Blöchl, P. E., Jepsen, O., & Andersen, O. K. (1994). Improved tetrahedron method for Brillouin-zone integrations. *Physical Review B*, *49*(23), 16223.

[56] Monkhorst, H. J., & Pack, J. D. (1976). Special points for Brillouin-zone integrations. *Physical review B*, *13*(12), 5188-5192.

[57] Motornyi, O., Raynaud, M., Dal Corso, A., & Vast, N. (2018, December). Simulation of electron energy loss spectra with the turboEELS and thermo_pw codes. In *Journal of Physics: Conference Series* (Vol. 1136, No. 1, p. 012008). IOP Publishing.

[58] Voigt, W. J. T. L. (1928). A determination of the elastic constants for beta-quartz lehrbuch de kristallphysik. *Terubner Leipzig*, *40*, 2856-2860.

[59] Hill, R. (1952). The elastic behaviour of a crystalline aggregate. *Proceedings of the Physical Society. Section A*, *65*(5), 349.

[60] Thirika A.M., Mulwa W.M., Makau N.W., Bamidele I.A (2022) *Ab Initio* Study of Structural and Vibrational Properties of Fe_2P-Type Materials for Near - Room - Temperature Refrigeration. *International Journal of Physics, 2022, Vol. 10, No. 1, 49-58*.

[61] Momma, K., & Izumi, F. (2011). VESTA 3 for three-dimensional visualization of crystal, volumetric and morphology data. *Journal of applied crystallography*, *44*(6), 1272-1276.

[62] Khuili, M., Fazouan, N., Abou El Makarim, H., Atmani, E. H., Rai, D. P., &Houmad, M. (2020). First-principles calculations of rare earth (RE= Tm, Yb, Ce) doped ZnO: Structural, optoelectronic, magnetic, and electrical properties. *Vacuum*, *181*, 109603.

[63] Khuili, M., El Hallani, G., Fazouan, N., Abou El Makarim, H., &Atmani, E. H. (2019). First-principles calculation of (Al, Ga) co-doped ZnO. *Computational Condensed Matter*, *21*, e00426.

[64] Chirchir G.K, Mulwa W.M. Bamidele I.A (2022) Structural, Electronic and Mechanical Properties of Re Doped FeMnP 0.67A0.33 (A=Ga and Ge): A DFT Study. *International Journal of Physics, 2022, Vol. 10, No. 1, 70-78.*

[65] Sarasamak, K., Limpijumnong, S., & Lambrecht, W. R. (2010). Pressure-dependent elastic constants and sound velocities of wurtzite SiC, GaN, InN, ZnO, and CdSe, and their relation to the high-pressure phase transition: A first-principles study. *Physical Review B*, *82*(3), 035201.

[66] Carlotti, G., Fioretto, D., Socino, G., & Verona, E. (1995). Brillouin scattering determination of the whole set of elastic constants of a single transparent film of hexagonal symmetry. *Journal of Physics: Condensed Matter*, *7*(48), 9147.

[67] Tyuterev, V. G., & Vast, N. (2006). Murnaghan's equation of state for the electronic ground state energy. *Computational materials science*, *38*(2), 350-353.

[68] Mbilo, M., Manyali, G. S., & Musembi, R. J. (2022). Ab initio study of $K_3Cu_3P_2$ material for photovoltaic applications. *Computational Condensed Matter*, *32*, e00726.

[69] Sun, J., Wang, H. T., He, J., & Tian, Y. (2005). Ab initio investigations of optical properties of the high-pressure phases of ZnO. *Physical Review B*, *71*(12), 125132.

[70] Azam, S., Irfan, M., Abbas, Z., Rani, M., Saleem, T., Younus, A., & Al-Sehemi, A. G. (2019). DFT study of the electronic and optical properties of ternary chalcogenides AlX_2Te_4. *Materials Research Express*, *6*(11), 116314.

[71] Vettumperumal, R., S. Kalyanaraman, and R. Thangavel. "Optical constants and near infrared emission of Er doped ZnO sol–gel thin films." *Journal of Luminescence* 158 (2015): 493-500.

[72] Liu, Y., Hou, Q., Sha, S., & Xu, Z. (2020). Electronic structure, optical and ferromagnetic properties of ZnO co-doped with Ag and Co according to first-principles calculations. *Vacuum*, *173*, 109127.

Copyright © 2024 The Author(s). Published by Scientific & Academic Publishing
This work is licensed under the Creative Commons Attribution International License (CC BY). http://creativecommons.org/licenses/by/4.0/